JOURNAL OF CATALYSIS **178,** 457–465 (1998)
ARTICLE NO. CA982160

NiMoS/γ-Al_2O_3 Catalysts: The Nature and the Aging Behavior of Active Sites in HDN Reactions

Liping Zhang,[1] Gurkan Karakas, and Umit S. Ozkan[2]

Department of Chemical Engineering, Ohio State University, Columbus, Ohio 43210

Received December 8, 1997; revised May 8, 1998; accepted May 14, 1998

The work presented in this paper is a continuation of our earlier work aimed at acquiring a fundamental understanding of sulfided Ni-Mo/γ-Al_2O_3 catalysts in HDN catalysis. A series of temperature-programmed desorption and reduction experiments were performed over *in-situ* sulfided bare γ-alumina support, alumina-supported monometallic Ni, Mo, and bimetallic NiMo catalysts. The TPD and TPR results were linked to the active site assignment of Ni- and Mo-associated centers in HDN reactions. Postreaction XPS and SEM characterizations were performed for catalysts used in HDN for up to 1000 h. One of the major changes during the aging of the Ni-Mo/γ-Al_2O_3 catalysts was the loss of some active sites associated with the Ni promoters. The decreased Ni content over the catalyst surface was consistent with the observed decrease in the hydrogenation function of the catalyst. Two possible mechanisms are suggested for the loss of Ni active sites. One is coking that spreads from the alumina support to the nickel sites. Another is segregation of some Ni atoms from the Ni-Mo-S structure due to loss of structural sulfur.

Key Words: **active sites; aging; supported NiMo sulfide; TPD; TPR; XPS; SEM; hydrodenitrogenenation; indole; H_2S.**

INTRODUCTION

In recent years, hydrodenitrogenation (HDN) catalysis has been gaining importance due to growing environmental concerns and an increasing need for processing heavy oils and low-quality stocks which contain larger quantities of nitrogen compounds than the traditional petroleum stocks. The work presented in this paper is a continued effort of this group in acquiring a fundamental understanding of sulfided Ni-Mo/γ-Al_2O_3 catalysts in HDN catalysis (1–5). Previously, we have reported our findings in the job distribution of Ni- and Mo-associated active sites and the role of feed sulfur compounds in the HDN of pyridine (1–3), indole and o-ethylaniline (OEA) (4–5). In this paper, we present additional studies on the characterization of active sites of supported NiMo sulfide catalysts and their aging behavior in the HDN of indole.

The conventional catalysts used in HDS and HDN processes are Co or Ni promoted MoS_2/Al_2O_3. CoMo catalysts are by far the most popular choice for desulfurization, whereas NiMo is often chosen when nitrogen removal is the primary process objective. However, unlike the extensive *in-situ* characterization done for HDS reactions over Co-Mo/Al_2O_3 catalysts, which has led to a fairly thorough understanding of the structure and catalytic mechanisms at the atomic and molecular level (6), less research has been done on characterizing the working mechanism of Ni-Mo sulfide catalysts under practical HDN reaction conditions. It is partly due to the fact that HDN reactions are more complex and more difficult to catalyze than HDS (6–11). HDN reactions usually consist of many intermediate aromatic ring hydrogenation and C-N bond cleavage steps which require a balanced dual functionality from the catalysts (5–9).

A common problem associated with heterogeneous catalysts is the decrease in activity and the change in selectivity with the age of the catalysts. As for metal sulfide hydrotreating catalysts, there have seen studies on deactivation (6 and references therein, 12–19), but little is reported on the changes of selectivity with catalyst aging, although the latter has an important impact on the HDN performance and the economy of the catalysts (20–22). Therefore, this study has been focused on the aging behavior of active sites of NiMoS/γ-Al_2O_3 catalysts and the corresponding product selectivity changes during HDN/HDS reactions of model compounds.

Polycyclic nitrogen compounds having both carbocycles and five- or six-membered heterocycles are the major nitrogen-containing species in petroleum feedstocks. Indole and quinoline are typical model compounds representative of the five-membered and six-membered polycyclic nitrogen species, respectively. While five-membered nitrogen heterocycles account for about 2/3 of total nitrogen content in petroleum crude (6), the majority of HDN studies have been conducted with quinoline (7–11, and references therein) and reports on indole are fewer and less extensive. Therefore, indole was chosen as the model compound in the work presented in this paper.

In industrial hydrotreating processes, sulfur compounds are almost invariably present. HDN feedstocks always

[1] Current address: Technical Center, Union Carbide Corporation, P.O. Box 8361, South Charleston, WV 25303.

[2] To whom correspondence should be addressed. E-mail: ozkan.1@osu.edu.

0021-9517/98 $25.00

contain sulfur compounds and a minimum partial pressure of H_2S is required to maintain catalysts in the fully sulfided condition and, hence, to obtain maximum catalyst activity (7). Therefore, the reaction studies of indole were performed over NiMoS/γ-Al_2O_3 catalysts in the presence of H_2S or benzothiophene (BT) with a wide range of operating temperatures, pressures, and times on-stream. Postreaction characterization of the catalysts which were on-stream for up to 1000 h was performed by using XPS and SEM without air exposure.

In order to better understand the nature of the active sites over NiMoS/γ-Al_2O_3 catalysts, a series of temperature-programmed reduction experiments were performed over *in-situ* sulfided bare γ-alumina support, alumina-supported monometallic Ni, Mo, and bimetallic NiMo catalysts. The results from our TPD, TPR, reaction studies, and postreaction characterizations are combined to gain insight on the nature and the aging behaviors of the active sites over NiMoS/γ-Al_2O_3 catalysts.

EXPERIMENTAL

Alumina-supported catalysts with different Ni and Mo loadings were prepared by wet co-impregnation of γ-Al_2O_3 with aqueous solutions of ammonium heptamolybdate and nickel nitrate. The preparation procedures and some characterization results were presented previously (1, 2). The catalyst compositions are reported as weight percentages of the oxide precursors, i.e., MoO_3, NiO, following the convention commonly used in HDS literature. The BET surface area of the catalysts used in these studies varied between 165 and 195 m^2/g, with pure alumina giving the highest surface area at 195 m^2/g.

Temperature-Programmed Desorption and Reduction

TPD/TPR experiments were performed using a built-in-house apparatus which was previously described (23). The reactor effluent composition was continuously monitored as a function of sample temperature by a mass spectrometer (Hewlett-Packard, MS Engine 5989A). For each of the TPD or TPR runs, 200 mg of sample was loaded in the reactors. All samples were sulfided *in-situ* using the same procedure as in reaction studies, i.e., flowing 10% H_2 in H_2S for 10 h at 400°C. In TPD experiments, the *in-situ* sulfided samples were cooled down to 25°C under the flow of the same sulfiding mixture. After being flushed with helium for 30 min, the samples were heated to 850°C at a rate of 5°C/min under a 50 cm^3(STP)/min helium flow.

In H_2 TPR experiments, the *in-situ* sulfided samples were flushed with 50 cm^3(STP)/min of He at 400°C for 30 min and then heated up to 500°C. After being degassed at 500°C for 1 h and cooled down to 25°C under vacuum, the samples were heated at 5°C/min from 25 to 950°C and kept at 950°C for 30 min. The reducing agent was 10% H_2 in He with a total flow rate of 55 cm^3(STP)/min.

HDN Reaction Studies

Catalytic reaction studies were carried out in a stainless steel flow system equipped with mass flow controllers for accurate flow delivery and on-line gas chromatography for feed and product stream analysis. The fixed-bed reactor was made out of 4-mm ID stainless steel tubing. The ends of the reactor tube were equipped with isolation valves to allow removal of the reactor tube from the reaction system and air-free transfer to the XPS and SEM apparatus. The total surface area of the catalyst in the reactor was kept constant at 50 m^2 which gave a catalyst bed length of ca 6 mm. Prior to all reaction studies, the catalysts were sulfided *in situ* at 400°C with 10% H_2 in H_2S for 10 h.

To study the aging behavior of NiMo sulfide catalysts in HDN/HDS reactions, two sets of 1000-h HDN/HDS runs were performed over the 3% NiO-15% MoO_3/γ-Al_2O_3 catalyst. The standard condition for the first run was 0.023% indole plus 0.023% H_2S in 60 cm^3(STP)/min of H_2 at 320°C and 100 psig. The standard condition for the second run was 0.046% indole plus 0.46% H_2S in 300 cm^3(STP)/min of H_2 at 320°C and 1000 psig. These two standard conditions were chosen to obtain similar and stable indole conversion levels (around 90%) at the early stages of the catalyst life. The very different H_2S concentrations for the 100 psig and 1000 psig tests were determined experimentally to be the minimum H_2S flow required for maintaining a stable indole HDN activity and a stable product distribution (demonstrated in Fig. 6 of Ref. [5] for P = 1000 psig). It should be mentioned that, during these 1000-h runs, the temperature and feed composition were varied on purpose for some short time periods for indole reaction kinetic studies or simultaneous indole HDN/BT HDS studies.

To characterize the NiMo catalysts at the early stages of their life, short-run indole HDN experiments were conducted over the 3% NiO-15% MoO_3/γ-Al_2O_3 and 20% MoO_3/γ-Al_2O_3 catalysts, as well as over the pure γ-Al_2O_3, in the absence or presence of BT. The on-stream time was 50 h and the operating procedures were identical in all these experiments. The starting reaction temperature was 200°C and was increased to a final temperature of 400°C with increments of 40°C. The concentrations for indole and BT in the feed were 0.023% each in 60 cm^3(STP)/min hydrogen. The reaction pressure was 100 psig. For convenience, a short-hand notation is assigned to each catalyst. Table 1 lists the notation and the description of the corresponding catalysts.

Postreaction XPS and SEM/EDXA Characterizations

The X-ray photoelectron spectrometer used for this work was V.G. ESCALAB Mark II, operated at 14 kV and 20 mA

TABLE 1

Notation and Description of the Catalysts

Notation	Description of the catalyst
NiMo-S	3% NiO–15% MoO_3/Al_2O_3 after sulfidation (prereaction)
NiMo-1000 LP	3% NiO–15% MoO_3/Al_2O_3 after 1000 h HDN in the presence of H_2S or benzothiophene at 100 psig
NiMo-1000 HP	3% NiO–15% MoO_3/Al_2O_3 after 1000 h HDN in the presence of H_2S at 1000 psig
NiMo-50 N	3% NiO–15% MoO_3/Al_2O_3 after 50 h HDN in the absence of sulfur compounds at 100 psig
NiMo-50 NS	3% NiO–15% MoO_3/Al_2O_3 after 50 h simultaneous HDN/HDS of indole/benzothiophene at 100 psig
Mo-50 NS	20% $MoO_3Al_2O_3$ after 50 h simultaneous HDN/HDS of indole/benzothiophene at 100 psig

with Mg Kα radiation (1253.6 eV). Binding energies were referenced to Al 2p of 74.4 eV. The SEM instrument used in this study was a Phillips XL30 Field Emission Scanning Electron Microscope with energy dispersive X-ray analysis (EDXA) capability. It was operated at 25 kV when performing the compositional analysis.

Postsulfidation and postreaction XPS and SEM/EDXA analyses were done without exposure to the atmosphere. Catalysts were flushed with helium at 400°C for 30 min and then cooled to room temperature under He flow. The catalysts were then sealed with valves located at both ends of the reactor tube. The reactors were taken to an argon-atmosphere glove box, where the catalysts were removed and mounted on the XPS or SEM sample holders. The samples were then transferred to the XPS or SEM chamber without exposure to air.

RESULTS AND DISCUSSIONS

Temperature-Programmed Desorption and Temperature-Programmed Reduction Studies

Figure 1 presents the H_2S TPD profiles over the γ-Al_2O_3 support, 20% MoO_3, and 3% NiO–15% MoO_3 catalysts after sulfidation. There are two major desorption peaks for each sample, with the first temperature maximum, which corresponds to physisorbed H_2S, appearing at 70°C for all samples. The maximum of the second H_2S desorption peak was at 482 and 490°C for the monometallic Mo and bimetallic Ni-Mo catalysts, respectively. The γ-Al_2O_3 support, however, showed a much lower desorption temperature at 200°C for the second H_2S peak. This observation suggests that the H_2S signal obtained for the Mo and Ni-Mo catalysts during the high temperature feature (second desorption peak) is mainly due to the desorption of H_2S from the catalyst and not from the support. It can be further envisioned that the desorbed H_2S molecules were from Mo-associated sites only since, other than a small difference in the desorption peak maximum temperature, the H_2S TPD profiles for the Mo and Ni-Mo catalysts were very similar.

Based on the TPD results, a degassing treatment at 500°C was performed prior to the H_2 TPR of the sulfided catalysts in order to remove all the adsorbed H_2S species. Therefore, it is expected that any H_2S that evolves during the TPR experiment is indeed from reduction.

The TPR profiles for the bare alumina support and the mono and bimetallic catalysts are presented in Figs. 2 and 3. The TPR profiles for the bimetallic Ni-Mo/γ-Al_2O_3 catalysts were quite different from those of the monometallic Ni/γ-Al_2O_3 and Mo/γ-Al_2O_3 catalysts. However, bimetallic Ni-Mo/γ-Al_2O_3 catalysts with different Ni loadings showed very similar profiles (Fig. 3). The very small H_2S peaks and the different peak temperatures for the alumina support on Fig. 2 indicate that the H_2S evolution for the monometallic Mo, Ni, and bimetallic Ni-Mo catalysts were resulted from the reduction of the catalysts.

An examination of the first reduction feature in Figs. 2 and 3 for the Mo and bimetallic Ni-Mo catalysts indicates that it may correspond to the removal of sulfur from the Mo sites because the peak occurs at the same temperature (around 160°C) for all Mo-containing catalysts. It also implies that Mo is in the same phase structure in both monometallic Mo and bimetallic Ni-Mo catalysts.

The second low-temperature H_2S peak at ca 210°C for the Ni-Mo catalysts could be due to the removal of sulfur from Ni centers in the Ni-Mo-S phase. The fact that the H_2S evolution peak for the monometallic Ni catalyst had a significantly higher peak maximum temperature (at around 270°C) also supports our suggestion that the second signal

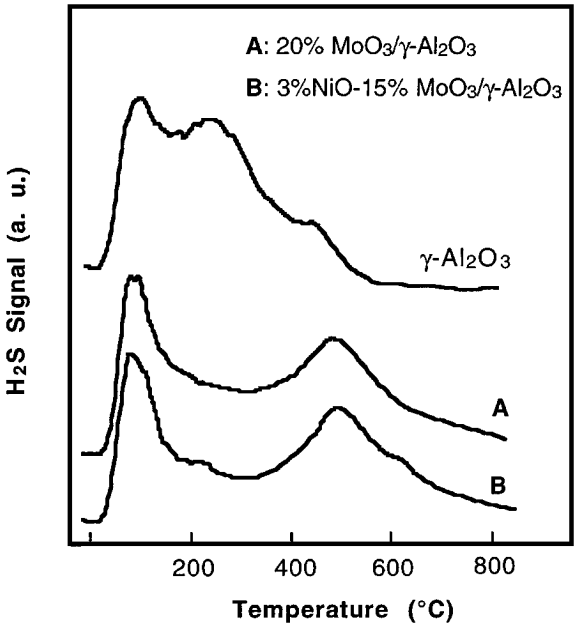

FIG. 1. H_2S TPD profiles of sulfided samples: pure γ-Al_2O_3, 20% MoO_3/γ-Al_2O_3, and 3% NiO–15% MoO_3/γ-Al_2O_3.

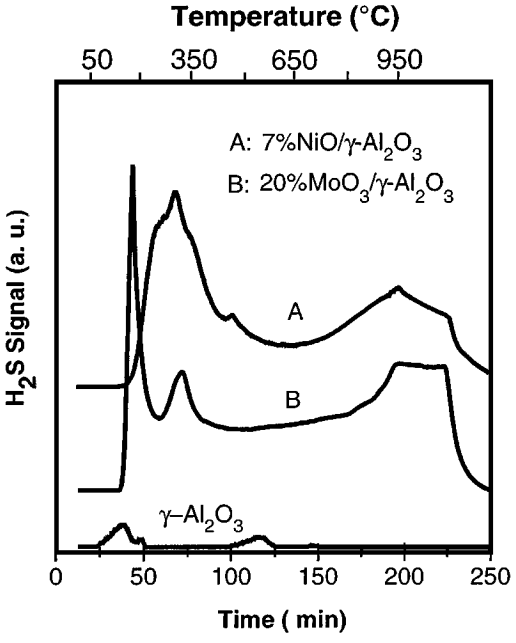

FIG. 2. H_2 TPR profiles of sulfided samples: pure γ-Al_2O_3, 20% MoO_3/γ-Al_2O_3, and 10% NiO/γ-Al_2O_3.

in the bimetallic catalysts is not due to a bulk nickel sulfide phase, but due to Ni centers in the Ni-Mo-S structure. The ratio of H_2S peak areas for the first and second features was slightly larger than 1 for the 3% NiO–15% MoO_3/γ-Al_2O_3 catalyst and about 1 for the 5% NiO–15% MoO_3/γ-Al_2O_3 and 7% NiO–15% MoO_3/γ-Al_2O_3 catalysts. It is conceivable that these two peaks correspond to the formation of sulfur vacancies on the edge planes of Ni-Mo-S phase. The 1 : 1 ratio for the Mo- and Ni-associated S vacancies for catalysts with high Ni loadings is in agreement with the maximum Ni accessibility to the MoS_2 plane that is concluded in the literature (6, 25). It is possible that the high-temperature features (300–450°C) observed in the TPR profiles may be indicative of the different Mo-S and Ni-S bond strengths of corner, singly-bonded, and doubly-bonded S sites. The identification of the high temperature features from the monometallic Ni, Mo, and bimetallic Ni-Mo catalysts, however, is difficult without the aid of other characterization techniques.

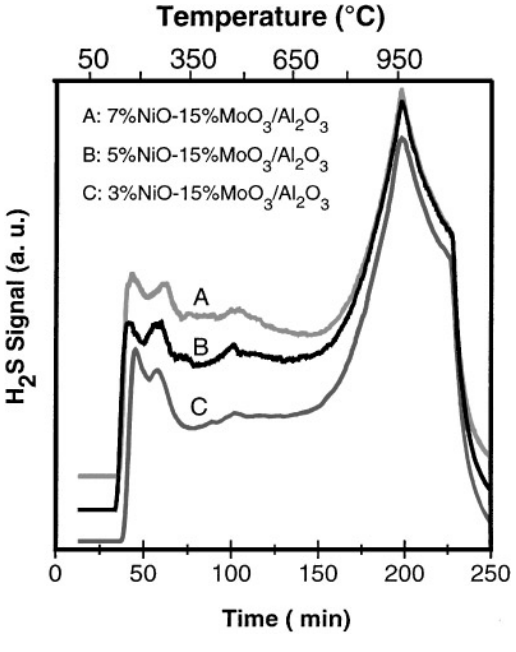

FIG. 3. H_2 TPR profiles of sulfided Ni-Mo/γ-Al_2O_3 catalysts with different Ni loading.

Based on some findings in the literature (24–34) and the results of our previous characterization and pyridine HDN studies, we have proposed that (2) there are two major types of active sites promoting HDN of nitrogen heterocycles over supported NiMo sulfides:

Type I. These are hydrogenation sites consisting of sulfur vacancies associated with Mo (type Ia sites) or Ni in Ni-Mo-S phase (type Ib sites). The intrinsic activity of type Ib sites are much higher than that of type Ia sites, such that the former is responsible for most of the hydrogenation activity.

Type II. These are C-N bond hydrogenolysis sites consisting of Brönsted acid centers associated with Mo atoms only. The adsorption and dissociation of an H_2S molecule can convert a sulfur vacancy to a Brönsted acid site and a sulfhydryl group (SH), but the adsorption is readily reversible if H_2S is removed from the reaction system.

The formation of the proposed active sites can be visualized through the following schemes:

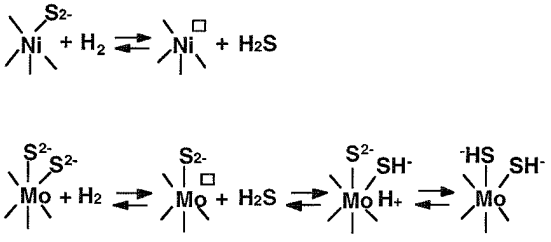

It is conceivable that the TPD and TPR results can be linked to the formation of these two types of active sites as shown in Table 2. The TPD feature that starts around 300°C signals the desorption and reassociation of H^+ and SH^- group from Brönsted acid sites. Since this is a reversible step, the basic role of H_2S in the HDN catalytic scheme is then envisioned to be to help maintain an optimum population of Brönsted acid sites (type II sites). It should be noted that there may be alternative interpretations of the TPD data. We cannot, for example, rule out the possibility that the H_2S evolved during TPD could be from the strongly adsorbed H_2S or from two SH groups on the same or neighboring Mo sites as suggested earlier (35).

TABLE 2

Summary of TPD and TPR Results over Sulfided Catalysts in Terms of the Proposed Active Site Model

H_2S from TPD		Temperature (°C)	
		T_{onset}	T_{max}
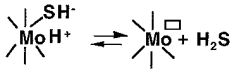	20%MoO_3/γ-Al_2O_3	300	482
	3%NiO-15%MoO_3/γ-Al_2O_3	300	490
H_2S from TPR			
		T_{onset}	T_{max}
	20%MoO_3/γ-Al_2O_3	160	194
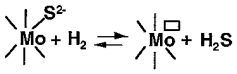	3%NiO-15%MoO_3/γ-Al_2O_3	155	185
	5%NiO-15%MoO_3/γ-Al_2O_3	150	175
	7%NiO-15%MoO_3/γ-Al_2O_3	158	180
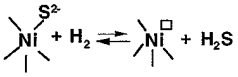	3%NiO-15%MoO_3/γ-Al_2O_3 1	220	260
	5%NiO-15%MoO_3/γ-Al_2O_3	200	270
	7%NiO-15%MoO_3/γ-Al_2O_3	210	290

The low-temperature H_2S signals observed in the hydrogen TPR experiments are, on the other hand, suggested to be related to the formation of sulfur vacancies by reaction of hydrogen with sulfur that is attached to Mo or Ni centers. It should be noted that the formation of Ni-associated sulfur vacancies (type Ib sites) takes place at a higher temperature (200–220°C) than the formation of Mo-associated sulfur vacancies (type Ia sites) (150–160°C). It should also be noted that the temperature required for the formation of the intrinsically more active type Ib sites corresponds to the lower end of the typical industrial hydrotreating temperatures. It should be noted that the sulfur-vacancy population attained in TPR experiments cannot be taken as a direct measure of the "steady-state" abundance of S vacancies in the presence of feed sulfur compounds since this "steady-state" population shoud be a function of the gas phase concentration of H_2S.

Reaction Studies

Ethylcyclohexane (ECH) and ethylbenzene (EB) were the major products from indole HDN. Since ECH is produced from complete hydrogenation of the benzene ring of indole whereas EB is mainly originated via the route involving the hydrogenolysis of indoline to *o*-ethylaniline (4, 5), the changes in the production rate of ECH and EB could reflect the changes in the relative strength of the hydrogenation and hydrogenolysis functions of the NiMo sulfide catalysts.

The production rates of ECH and EB from indole HDN vs on-stream time were plotted in Fig. 4 for the two 1000-h tests which were performed over the 3% NiO–15% MoO_3/γ-Al_2O_3 catalysts under either 100 psig (NiMo-1000 LP) or 1000 psig (NiMo-1000 HP) total pressure. As shown in Fig. 4, the ECH production rate decreased with increasing on-stream time for both NiMo-1000 LP and NiMo-1000 HP catalysts. The EB production rate, on the other hand, appeared to be unchanged throughout 1000-h reaction period in both tests. Since the hydrogenation function is mainly performed by Ni-associated active sites and the hydrogenolysis function is related to the Mo-associated active sites (1, 2, 4), the results in Fig. 4 imply that the Ni-associated active sites are deactivating with the aging of the catalyst, whereas Mo-associated active centers are almost unaffected.

Postreaction XPS and SEM/EDXA

Figure 5 shows the XPS spectra of the Mo 3d–S 2s region for the sulfided 3% NiO–15% MoO_3/γ-Al_2O_3 catalyst before and after HDN/HDS reactions up to 1000 h. It is seen that the shape and the intensity of the spectra for the

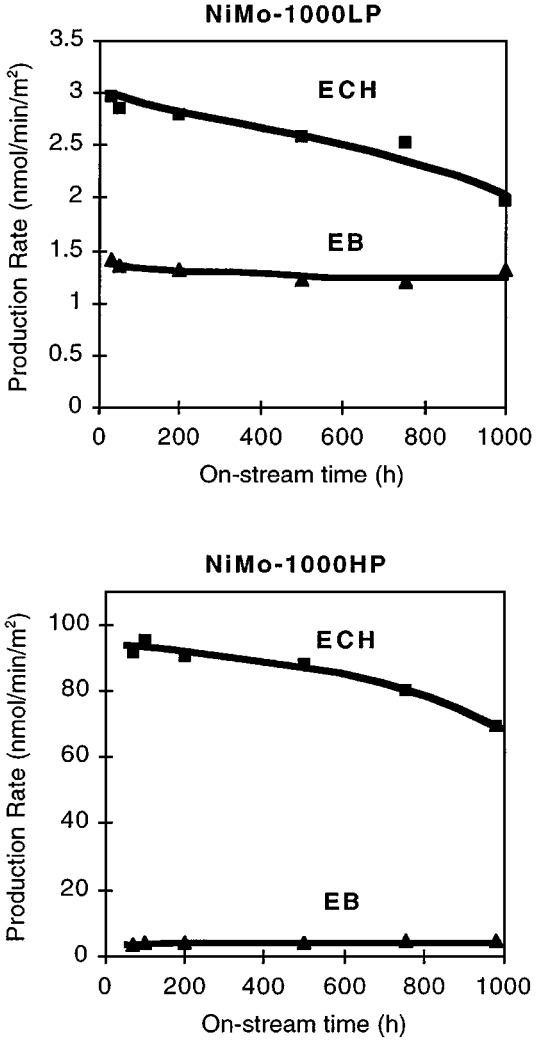

FIG. 4. Change of ECH and EB production rates with on-stream time from indole HDN in the presence of H_2S over the NiMo-1000 LP and NiMo-1000 HP catalysts under standard reaction conditions.

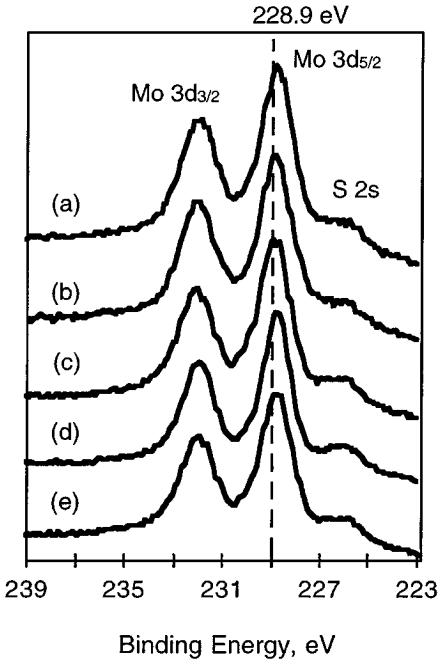

FIG. 5. XPS spectra of the Mo 3d–S 2s region of sulfided 3% NiO-15% MoO_3/γ-Al_2O_3 catalysts: (a) NiMo-1000 HP, (b) NiMo-1000 LP, (c) NiMo-50 N, (d) NiMo-50 NS, (e) NiMo-S.

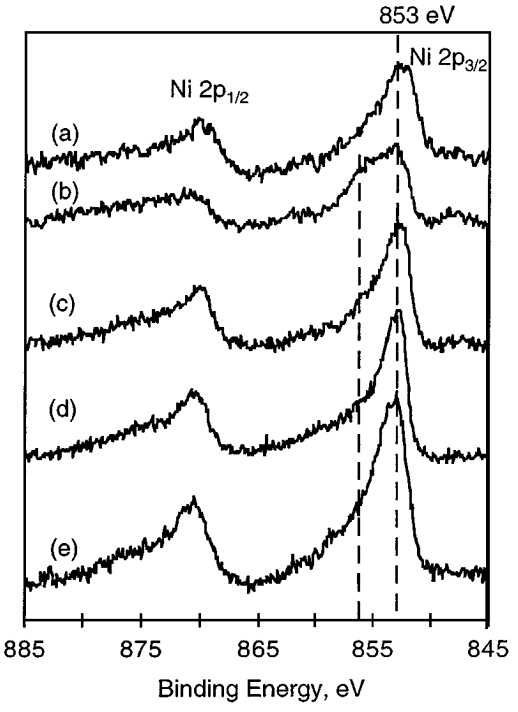

FIG. 6. XPS spectra of Ni 2p region of the 3% NiO–15% MoO_3/γ-Al_2O_3 catalysts: (A) NiMo-1000 HP, (B) NiMo-1000 LP, (C) NiMo-50 N, (D) NiMo-50 NS, (E) NiMo-S.

catalysts subjected to different on-stream times and different reaction conditions did not show pronounced differences from that of the prereaction catalyst. Both the Mo $3d_{5/2}$ binding energy (228.9 eV) and the shape of each spectrum are characteristic of a typical MoS_2 structure.

The Ni 2p spectra for the same set of catalysts are shown in Fig. 6. Generally, the Ni $2p_{3/2}$ binding energy for each of the catalysts was the same at ca 853 eV, which corresponds to the Ni in Ni-Mo-S structure (2). However, the intensity of the Ni 2p signal was substantially lower for both of the 1000 hour-on-stream catalysts than for the prereaction sulfide, indicating a loss of Ni from the catalyst surface. The decrease in Ni signal intensity was also apparent for the two short-run catalysts.

From Fig. 6, it was also observed that a feature around 856.3 eV which corresponds to $NiAl_2O_4$ (2) appeared for the NiMo-1000 LP catalyst with a significant intensity. The presence of the $NiAl_2O_4$ phase was also visible for the NiMo-50 N catalyst. Since the NiMo-50 N catalyst was used for indole HDN in the absence of sulfur compounds, this observation suggests that the appearance of the $NiAl_2O_4$ phase could be due to the loss of sulfur atoms which are needed to maintain the Ni-Mo-S structure.

When the Ni Auger lines for the pre- and postreaction catalysts are compared, the loss of Ni from the catalyst surface was evidenced again, as shown in Fig. 7. The Ni Auger signal is much more surface sensitive than the Ni 2p signal so that it only reflects the change of Ni in the top 1 or 2 layers of the catalyst surface. As seen in Fig. 7, the intensity of the Ni Auger signal (around 407 eV) of the NiMo-50NS catalyst was apparently lower than that of the prereaction catalyst. The decrease in the Ni Auger signal intensity for the two 1000 hour-on-stream catalysts was even more pronounced (the spectra for the two catalysts were almost identical therefore only that of NiMo-1000 LP was

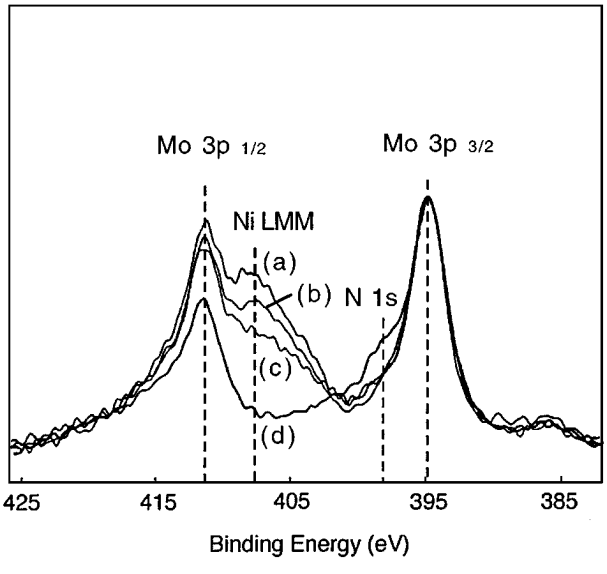

FIG. 7. XPS spectra of Mo 3p–Ni LMM-N 1s region of the sulfide catalysts: (A) NiMo-S, (B) NiMo-50 NS, (C) NiMo-1000 LP, (D) Mo-50 NS.

shown in Fig. 7). Combining the results in Figs. 6 and 7, it could be concluded that some Ni atoms disappeared from the surface of Ni-Mo catalysts, even over a short on-stream time period. The loss of surface Ni atoms increased with increasing on-stream time.

There is also a feature around 397 eV on the postreaction monometallic Mo catalyst, which can be due to N 1s signal (Fig. 7). When this signal is compared between the postreaction Mo and Ni-Mo catalysts, the former showed a nitrogen accumulation over the surface, while the latter did not. A similar N 1s peak was also observed over pure alumina support after it was exposed to the HDN/HDS media. It is possible that the N 1s signal is due to irreversible adsorption of organonitrogen compounds on the alumina support. The fact that this signal appears only on the monometallic Mo catalyst and not on the bimetallic catalyst may be explained by the better dispersion of Mo in the bimetallic catalyst (2). The formation of a surface Mo-nitride layer also remains as a possibility, but there is not enough evidence to accept or to rule out this possibility with the present data.

Table 3 shows the atomic ratios of Ni/Mo, S/Mo, and Al/Mo for the Ni-Mo catalysts compared above, obtained from XPS measurements. The calculation was based on the integrated peak intensities of Ni $2p_{3/2}$. Mo $3d_{5/2}$, S 2p, and Al 2p corrected by the atomic sensitivity factors. The normalized ratios are also included to make the comparison easier. The normalization is done by dividing the actual ratio by that of the freshly sulfided catalyst so that the normalized ratio value for the freshly sulfided catalyst is unity. The post-reaction catalysts NiMo-1000 LP and NiMo-1000 HP showed a decrease of 44 and 37%, respectively, in the relative Ni signal compared to the freshly sulfided catalyst. Even after an on stream time of only 50 h, the normalized nickel signal decreased by 28%. The decrease in the S and Al signals, on the other hand, were significantly lower between 9 and 17%.

Among the postreaction catalysts, the NiMo-1000 HP had the smallest decrease in S and Al content. For this catalyst sample, the higher S/Mo ratio compared to other samples could be due to a higher H_2S concentration in the reaction feed. The higher Al/Mo ratio over the NiMo-1000 HP catalyst could be an indication of decreased carbon deposition over the alumina support under high H_2 pressures.

It should be pointed out that the XPS spectra of C 1s for all of the post-reaction catalysts showed a higher C content and some pronounced differences in the peak shape and binding energy. However, it was not possible to quantify the carbon content due to the fact that some of the carbon signals were from the double-sided tape that was used to mount the catalyst to the XPS sample holder.

From SEM experiments, average S/Mo and Ni/Mo atomic ratios are calculated based on EDXA analysis obtained from several randomly selected particles. Mo L, S K, and Ni K lines were used in the calculation. The EDXA results for the freshly sulfided (NiMo-S) and postreaction (NiMo-1000HP) catalysts are plotted in Fig. 8, together with the results from XPS measurements. In contrast to the XPS results, both the S/Mo and Ni/Mo ratios obtained from SEM-EDXA showed very little difference between the pre- and postreaction catalysts. Since EDXA is not a surface-sensitive technique, the SEM-EDXA results indicate that the bulk Ni-Mo-S composition remains the same. The Ni/Mo ratios obtained from SEM-EDXA were close to the theoretical value expected for the catalyst composition of 3% NiO–15% MoO_3/Al_2O_3.

The lower Ni/Mo and S/Mo ratios obtained in the XPS analysis of the postreaction catalysts indicates that the loss of nickel and sulfur are mainly from the surface. It should also be noted that the loss of Ni from the surface is much more pronounced than the loss of sulfur. Another interesting feature of this figure is that the XPS analysis gives a higher Ni/Mo ratio of the fresh catalyst than does the EDXA analysis. Again, this can be explained by the position of the nickel in the Ni-Mo-S structure, which is primarily on the edge planes of the MoS_2 slabs, hence leading to a higher Ni/Mo signal in the surface than in the bulk. One final point about this figure is that the S/Mo ratio in the XPS analysis for the fresh catalyst is lower than the S/Mo ratio obtained from EDXA analysis for both pre- and postreaction catalysts. This difference, however small, could be an indication of some sulfur vacancies already generated on the surface of the catalyst during pretreatment.

TABLE 3

Atomic Ratios of Ni/Mo, S/Mo, and Al/Mo for the Ni-Mo Catalyst from XPS Measurements

	XPS atomic ratio					
	Ni/Mo (normalized)		S/Mo (normalized)		Al/Mo (normalized)	
NiMo-S	0.48	(1.00)	1.990	(1.00)	6.623	(1.00)
NiMo-50 NS	0.35	(0.73)	1.751	(0.88)	5.882	(0.89)
NiMo-50 N	0.34	(0.72)	1.643	(0.83)	5.475	(0.83)
NiMo-1000 LP	0.27	(0.56)	1.646	(0.83)	5.650	(0.85)
NiMo-1000 HP	0.30	(0.63)	1.786	(0.90)	6.024	(0.91)

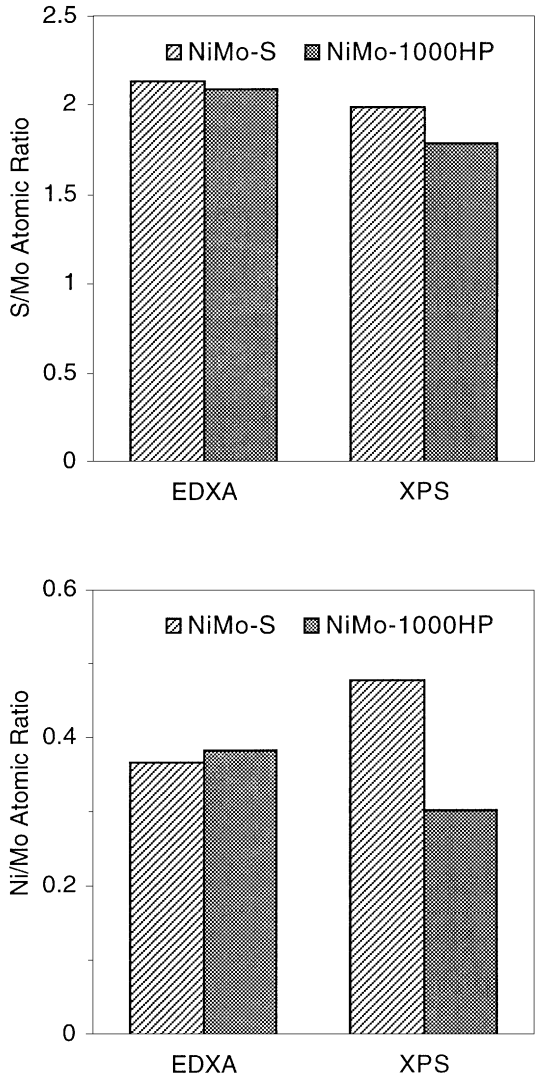

FIG. 8. Comparison of the S/Mo and Ni/Mo ratios obtained by SEM and XPS for the 3% NiO–15% MoO3/γ-Al_2O_3 catalysts.

Mechanisms for the Loss of Hydrogenation Activity

Combining the indole reaction studies with the postreaction XPS and SEM/EDXA characterization results, the loss of the hydrogenation activity of the NiMo catalysts can be related to the measured decrease of the Ni content over the catalyst surface. Since Ni is responsible for the hydrogenation activity, the loss in Ni-associated active sites leads to a decrease in the production of the saturated products.

There are two possible mechanisms accounting for the loss of Ni active sites, i.e., the spreading of carbon deposits which originate from the alumina support, and the segregation of Ni from the Ni-Mo-S active phase and bonding of Ni with the alumina support. First, Ni sites are more prone to being covered by carbon deposition since they are located on the edges of the MoS_2 slabs. Deactivation studies in the literature have confirmed that coking, that spreads from the alumina support to the active phase, is one of the major causes of the deactivation of sulfide catalysts (6, 15, 18). Second, loss of S in the Ni-Mo-S slabs may force the segregation of some Ni atoms from the Ni-Mo-S structure, as evidenced by the presence of $NiAl_2O_4$. It is highly likely that both of these mechanisms may be in effect during the course of catalyst deactivation.

The loss of Ni active species from the catalyst surface was fast in the initial period of the catalyst life. This is consistent with the well recognized fast coking of the catalyst at the initial period. Between the two 1000 hour-on-stream catalysts, the one operated at higher hydrogen pressures showed a higher surface Ni content than the one operated at 100 psig, despite the fact that it had processed much more N-containing feed. One possible explanation may be that higher hydrogen pressure could slow down the loss of Ni by decreasing the carbon deposition rate. A second explanation may be that for high H_2 pressure experiments (NiMo-1000 HP), a higher H_2S concentration was used to prevent sulfur depletion. Reduced S-depletion, in turn, could help maintain the Ni-Mo-S structure and prevent segregation of Ni from the N-Mo-S phase.

CONCLUSIONS

The TPR results presented in this paper suggest that Ni associated sulfur vacancies, which are responsible for hydrogenation reactions, are readily formed via the removal of sulfur by hydrogen at temperatures used in commercial HDS/HDN operations. The TPD results suggest that the Brönsted acid sites, which are responsible for C-N bond hydrogenolysis reactions, may be lost at temperature 300°C due to the easy desorption and reassociation of H^+ and SH^- to H_2S. The Brönsted acid sites can be replenished by the presence of H_2S in the gas phase since this step is reversible.

One of the major changes during the aging of the NiMoS/γ-Al_2O_3 catalysts is the loss of some active sites associated with the Ni promoters. This was evidenced by the significantly lower intensities of the Ni 2p and Ni auger signals, and the appearance of the inactive $NiAl_2O_4$ phase over the postreaction catalysts. The decreased Ni content over the catalyst surface was consistent with the observed decrease in the hydrogenation function of the catalyst.

Two possible mechanisms are suggested for the loss of Ni active sites. One is coking that spreads from the alumina support to the active phase. Since Ni sites are located on the edges of the MoS_2 slabs, they are more prone to being covered by carbon deposition. Another is segregation of some Ni atoms from the Ni-Mo-S structure. The segregation is possibly due to the loss of structural sulfur which bonded Ni to the Ni-Mo-S phase. It is conceivable that the role of sulfur compounds in the gas phase is not only to replenish the Brönsted acid sites, but also to prevent the segregation of Ni from the Ni-Mo-S active phase.

ACKNOWLEDGMENT

Financial support provided for this work by the National Science Foundation through Grant HRD-9023778, by TUBITAK-BAYG, and by the EXXON Education Foundation is gratefully acknowledged.

REFERENCES

1. Ozkan, U. S., Ni, S., Zhang, L., and Moctezuma, E., *Energy Fuels* **8**, 249 (1994).
2. Ozkan, U. S., Zhang, L., Ni, S., and Moctezuma, E., *J. Catal.* **148**, 181 (1994).
3. Ozkan, U. S., Zhang, L., Ni, S., and Moctezuma, E., *Energy Fuels* **8**, 831 (1994).
4. Zhang, L., and Ozkan, U. S., *Stud. Surf. Sci. Catal.* **101**, 1223 (1996).
5. Zhang, L., and Ozkan, U. S., *Stud. Surf. Sci. Catal.* **106**, 69 (1997).
6. Topsøe, H., Clausen, B. S., and Massoth, F. E., "Hydrotreating Catalysis." Springer-Verlag, Berlin, 1996.
7. Satterfield, C. N., "Heterogeneous Catalysis in Industrial Practice," 2nd Ed., Chap. 9, p. 383. McGraw–Hill, New York, 1991.
8. Perot, G., *Catal. Today* **10**, 447 (1991).
9. Ho, T. C., *Catal. Rev.-Sci. Eng.* **30**, 117 (1988).
10. Girgis, M. J., and Gates, B. C., *Ind. Eng. Chem. Res.* **30**, 2021 (1991).
11. Prins, R., *in* "Encyclopedia of Catalysis" (Knozinger, Ertl, and Weitkamp, Eds.), in press.
12. Diez, F., Gates, B. C., Miller, J. T., Sajkowski, and Kukes, S. G., *Ind. Eng. Chem. Res.* **29**, 1999 (1990).
13. Zeuthen, P., Blom, P., and Massoth, F. E., *Appl. Catal.* **78**, 265 (1991).
14. Hughes, A. E., Pratt, K. C., and Tsai, P., *Appl. Catal. A: General* **90**, 117 (1992).
15. van Doorn, J., and Moulijn, J. A., *Fuel Process. Technol.* **35**, 275 (1993).
16. Eijsbouts, S., Heinerman, J. J. L., and Elzerman, H. J. W., *Appl. Catal. A: General* **105**, 69 (1993).
17. Kim, C.-S., and Massoth, F. E., *Fuel Process. Technol.* **35**, 289 (1993).
18. Weissman, J. G., and Edwards, J. C., *Appl. Catal. A: General* **142**, 289 (1996).
19. Yokoyama, Y., Ishikawa, N., Nakanishi, K., Satoh, K., Nishijima, A., Shimada, H., Matsubayashi, N., and Nomura, M., *Catal. Today* **29**, 261 (1996).
20. Olalde, A., and Perot, G., *Appl. Catal.* **13**, 373 (1985).
21. Kasztelan, S., des Courieres, T., and Breysse, M., *Catal. Today* **10**, 433 (1991).
22. Katzer, J. R., and Sivasubramanian, R., *Catal. Rev.-Sci. Eng.* **20**, 155 (1979).
23. Ozkan, U. S., Cai, Y., Kumthekar, M. W., and Zhang, L., *J. Catal.* **142**, 182 (1993).
24. Topsøe, N.-Y., and Topsøe, H., *J. Catal.* **84**, 386 (1983).
25. Yang, S. H., and Satterfield, C. N., *J. Catal.* **81**, 168 (1983).
26. Yang, S. H., and Satterfield, C. N., *Ind. Eng. Chem. Process Des. Dev.* **23**, 20 (1984).
27. Topsøe, H., Clausen, B. S., Candia, R., Wivel, C., and Morup, S., *J. Catal.* **68**, 433 (1981).
28. Wivel, C., Candia, R., Clausen, B. S., Morup, S., and Topsøe, H., *J. Catal.* **68**, 453 (1981).
29. Alstrup, I., Chorkendorff, I., Candia, R., Clausen, B. S., and Topsøe, H., *J. Catal.* **77**, 397 (1982).
30. Topsøe, H., and Clausen, B. S., *Catal. Rev.-Sci. Eng.* **26**, 395 (1984).
31. Topsøe, H., Clausen, B. S., Topsøe, N.-Y., and Pedersen, E., *Ind. Eng. Chem. Fund.* **25**, 25 (1986).
32. Mcllvried, H. G., *Ind. Eng. Chem. Process Des. Dev.* **10**, 125 (1971).
33. Ledoux, M. J., *Appl. Catal.* **9**, 31 (1984).
34. Hadjiloizou, G. C., Butt, J. B., and Dranoff, J. S., *Ind. Eng. Chem. Res.* **31**, 2503 (1992).
35. Sieraalta, A., and Ruette, F., *J. Molec. Catal.* **109**, 227 (1996).
36. Massoth, F. E., and Zeuthen, P., *J. Catal.* **145**, 216 (1994).